CHAPTER IV

RESULTS AND DISCUSSION

4.1 Preparation of Na-Clay and Characterization

The received BNH has a white appearance. An impurity such as carbonate, quartz, feldspar, sand and other inorganic compound is present along with the received clay. As a non swellable portion, these impurities were separated by a combined gravity sedimentation and centrifugal sedimentation. According to Stoke's law, a larger particle settles faster than a smaller particle size, given the same density, in the same liquid. The gravitational sedimentation was carried out prior to a homoionic clay conversion in order to save some reagent. The sedimentation was achieved by leaving the clay suspension to settle overnight. The suspended clay in the supernatant liquid was slowly separated and dried for further treating into homo cationic clay.

Sodium ion was chosen as an interlayer cation due to its excellent swellability in water. A strongly hydrated sodium ion promotes a larger separation between each silicate layer, which facilitates the ion-exchanged reaction. Homoionic Na-montmorillonite was prepared by treating the pretreated clay with an excess sodium chloride solution. The suspension was stirred and left overnight to ensure a complete exchange reaction. Excess sodium ion was washed several times with deionized water and followed by dialysis against the water. It was done until no white precipitation of silver chloride was detected by silver nitrate solution, no more chloride. The clay was then dried and ready for particle size separation.

The particle size separation is done by centrifuge technique.[3] A condition for separation the pure mineral clay, particle size less than 2 mm, was calculated according to Stoke's law. For 150.0 mL suspension in 250 mL centrifuge tube, the separation particle size less than 2 mm is achieved at the speed of 750 rpm for 3.3 min. To ensure a good separation, the experiment is carried out at 800 rpm for 15 minutes.

The clay was reinvestigated for the non-clay portion by XRD. Figure 4.1 and Table 4.1 indicate that most of non clay mineral was removed. However a trace amount of cristobalite cannot be separated because it has a comparable specific gravity and particle size is close to the clay mineral.

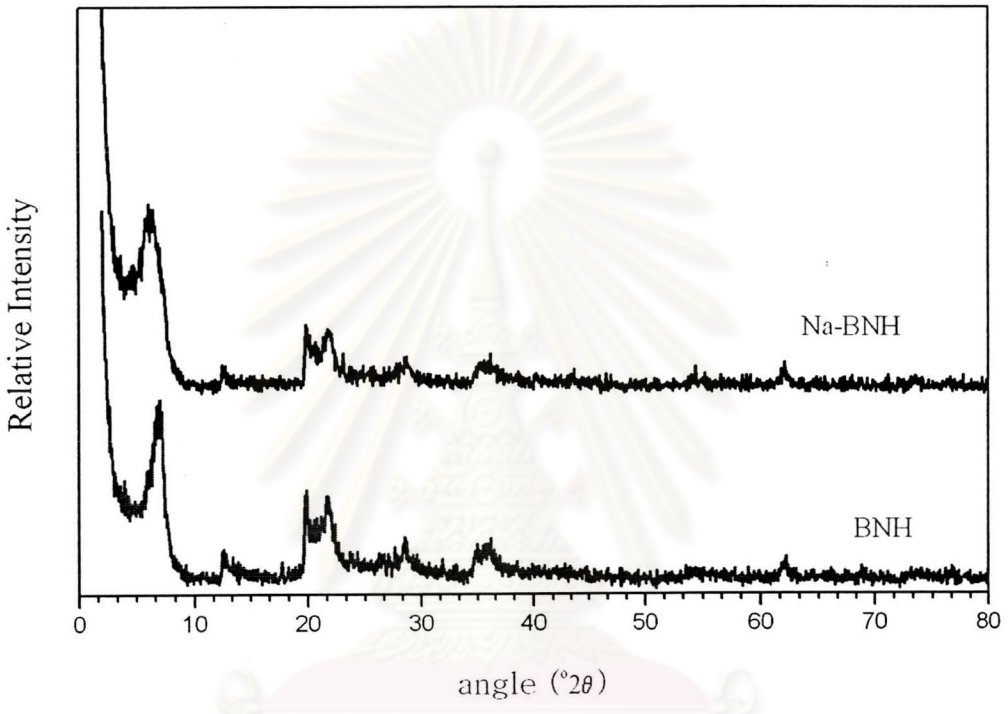

Figure 4.1 XRD patterns of received BNH and Na-BNH

Table 4.1. A composition XRD pattern of received BNH and Na-BNH

Angle (°2θ)		Identification
Received BNH	Na-BNH	
6.95	6.30	(001) Na-BNH
12.69	12.77	(002) Na-BNH
19.80	19.88	(110) Na-BNH
21.75	21.82	Cristobalite
28.53	28.61	Cristobalite
34.92	34.99	Cristobalite
62.16	61.99	(060) Na-BNH

The CEC represents the amount of the exchangable cation withheld in the clay interlayer. In this work, the CEC of Na-BNH was measured by methylene blue index[9] where the amount of methylene blue dye adsorbed by clay mineral was measured. The measured value depends on the specific surface of clay. The CEC for Na-BNH used in this study is 1.42 meq/g clay.

4.2 Preparation of Organoclay and Characterization

Na-BNH is used as a template for the organoclay preparation. Two major variables, the surfactant chemistry and the concentration of surfactant, will be investigated.

4.2.1 Effect of Surfactant Chemistry on the Interlayer Spacing of Clay

Three quaternary ammonium salts with different molecular architecture and chemical functionality are used in this study. They are tallowtrimethyl ammonium chloride (TTM), oleylmethylbis(2-hydroxyethyl) ammonium chloride (OMH) and octadecylmethyl[ethoxylate(15)] ammonium chloride (ODMH). The chemical structures of the ammonium salts are shown in Figure 4.2. The effect of the molecular architecture will be first discussed.

The structure of TTM consists of a long alkyl chain, 18 carbon atoms, with an estimated length of 20.3 Å. A molecular cross section, assuming the all *trans* configuration with the closed packing, is around 20.0 $Å^2$.

The second surfactant is OMH, which consists of a long alkyl chain, 18 carbon atoms, and two flexile ethoxy (ethoxide). The last surfactant is ODMH where the main component is the long alkyl chain, 18 carbon atoms, and two long ethylene oxide oligomers (ETO), 15 repeats. The length of alkyl chain is estimated to be 20.3 Å. The cross sectional area cannot be due to a flexibility of the ethylene oxide oligomer.

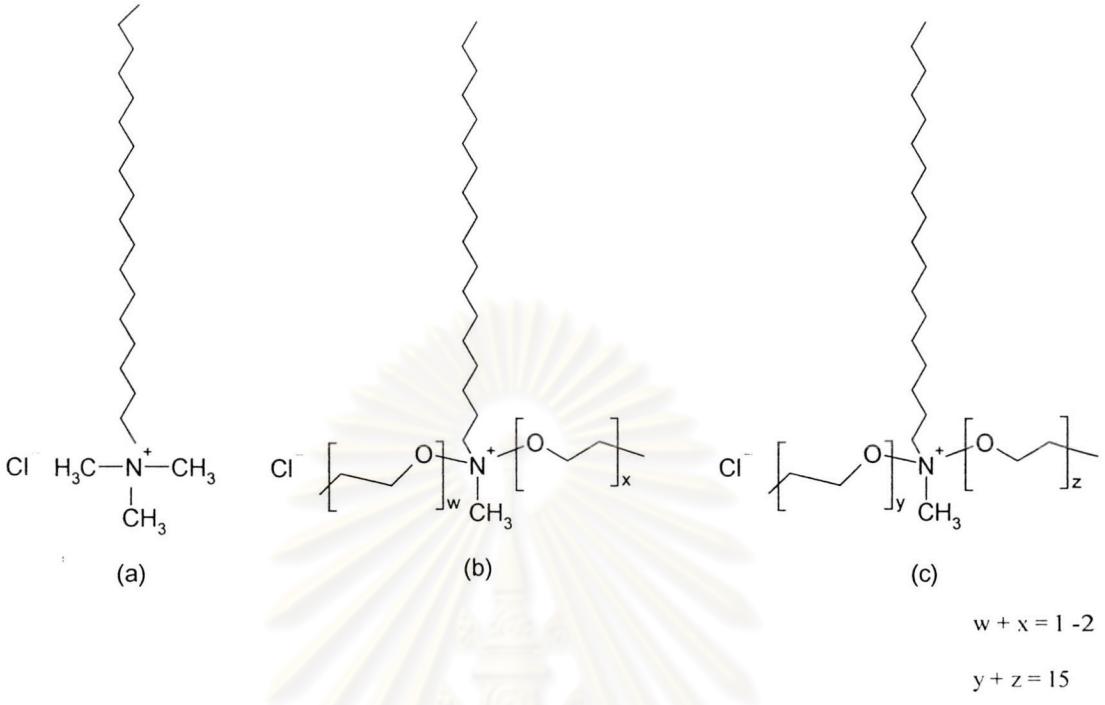

Figure 4.2 Structure of surfactant; (a) TTM, (b) OMH and (c) ODMH

The intercalation of silicate layer was followed by Fourier transform infrared spectrophotoscopy (FTIR) and X-ray diffraction (XRD).

4.2.1.1 FTIR

Na-BNH and organoclay were characterized by FTIR to verify the intercalation of surfactant into the interlayer of clay. FTIR spectra of Na-BNH and organoclay with 1.0 mmol surfactant concentration loading are shown in Figure 4.3 and Table 4.2.

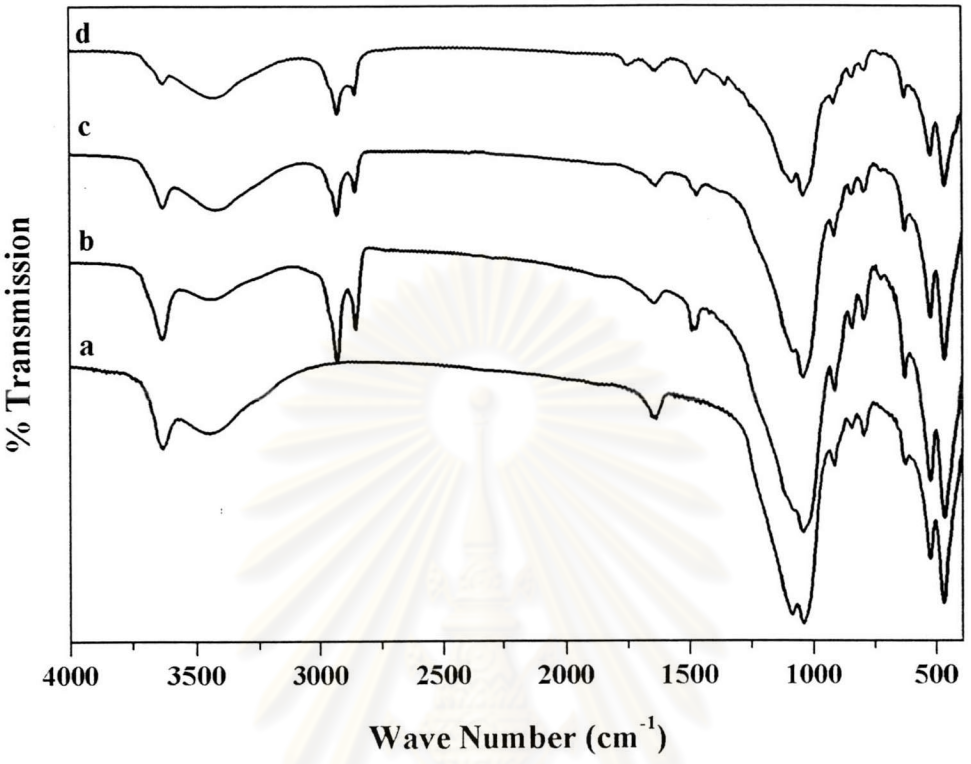

Figure 4.3 FTIR spectra of clay and organoclay with 1.0 mmol surfactant concentration loading; (a) Na-BNH, (b) TTM-BNH, (c) OMH-BNH and (d) ODMH-BNH

From the results, the specifically characteristic peak of the surfactant was shown in all organoclay's but not present in the Na-BNH. The Na-BNH shows their characteristic peak at 3628, 3434, 1037, 522 and 465 cm-1 which are associated with O-H stretching, O-OH stretching, Si-O stretching, Al-O stretching and Si-bending respectively (Table 4.2).

For BNH-TTM, the peak at 3632, 3442, 2929, 2854, 1479, 1041, 523 and 465 cm^{-1} can be assigned as the O-H stretching, O-OH stretching, C-H stretching of methyl and methylene group, CH_3 deformation, Si-O stretching, Al-O stretching and Si-O bending respectively. Similarly, OMH-BNH and ODMH-BNH exhibited the characteristic peak of BNH and surfactant like TTM-BNH. All of these characteristic peaks imply the success of the modifying of silicate layers.

Table 4.2 The infrared peaks assignment of Na-BNH, TTM-BNH, OMH-BNH and ODMH-BNH.

Assignment	Peak position (cm^{-1})			
	Na-BNH	TTM-BNH	OMH-BNH	ODMH-BNH
O-H stretching of BNH	3629	3632	3629	3628
O-OH stretching of BNH	3446	3442	3422	3431
C-H stretching of methyl group	-	2929	2929	2926
C-H stretching of methylene group	-	2854	2857	2860
CH_3 deformation	-	1479	1469	1468
Si-O stretching	1042	1041	1042	1038
Al-O stretching	522	523	523	523
Si-O bending	468	465	465	463

4.2.1.2 XRD

The XRD provides a strong evidence for the intercalation of quaternary ammonium cation into the clay interlayer. The XRD patterns of Na-BNH and organoclay are shown in Figure 4.4.

XRD peak of the organoclay is moving toward a lower 2θ angles relative to the Na-BNH. This indicates that the distance between silicate layers, d-spacing, is expanded due to the intercalated quaternary ammonium ion. The calculated peak positions and interlayer spacing are listed in Table 4.3.

The basal spacing of Na-BNA is 14.80 Å. After treatment with quaternary ammonium salt by ion-exchange reaction, the basal spacing of TTMBNH, OMHBNH and ODMH are 19.37, 21.07 and 33.89 Å, respectively.

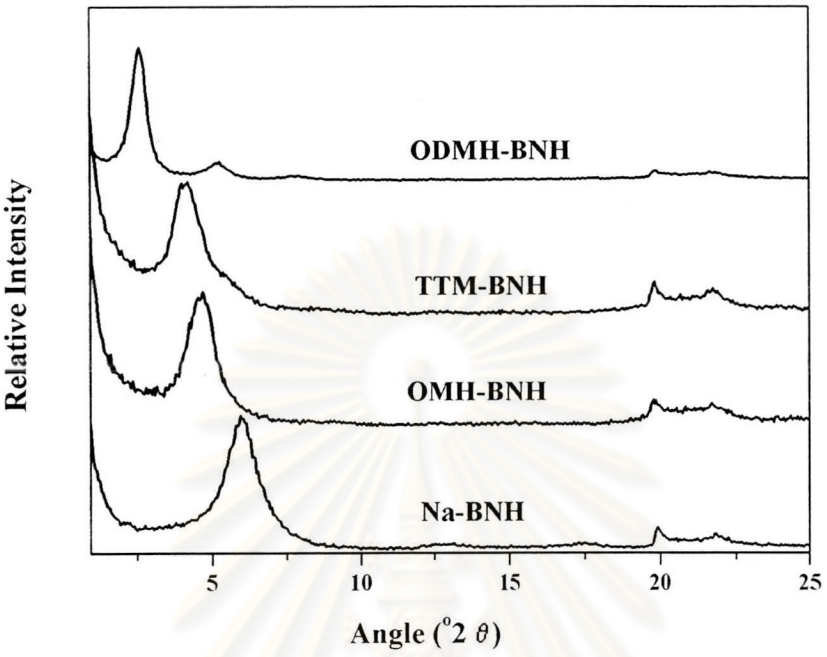

Figure 4.4 XRD patterns of Na-BNH, organoclay with 1.0 mmol sufactant concentration loading; OMH-BNH, TTM-BNH and ODMH-BNH.

Table 4.3 The basal spacing of Na-BNH and organoclay with 0.1 mmol surfactant concentration loading.

Surfactant-Clay	Angle (°2 θ)	Interlayer spacing (Å)	Δ d (Å)
Na-BNH	6.30	14.01	4.01
TTM-BNH	4.56	19.37	9.37
OMH-BNH	4.19	21.07	11.07
ODMH-BNH	2.60	33.89	23.89

4.2.2 Effect of the surfactant concentration loading on the interlayer spacing of clay

The effects of the surfactant concentration loading on the intercalation process were investigated. This was done in order to elucidate the effect of clay surface coverage and the surfactant uptake on the formation of organoclay. The surfactant concentrations used in this investigation are 0, 0.5, 1.0 and 1.5 mmol/g clay. Thermogravimetric analysis (TGA) was used to obtain the weight loss due to the interlayer cation.

The intercalation of organoclay at various surfactant loadings are shown in Figures 4.5-4.7 and Table 4.4. From the information, the interlayer spacing of all organoclay was increased due to the intercalation of the organic molecule. The amount of the intercalated surfactant is determined by the weight loss from the TGA.

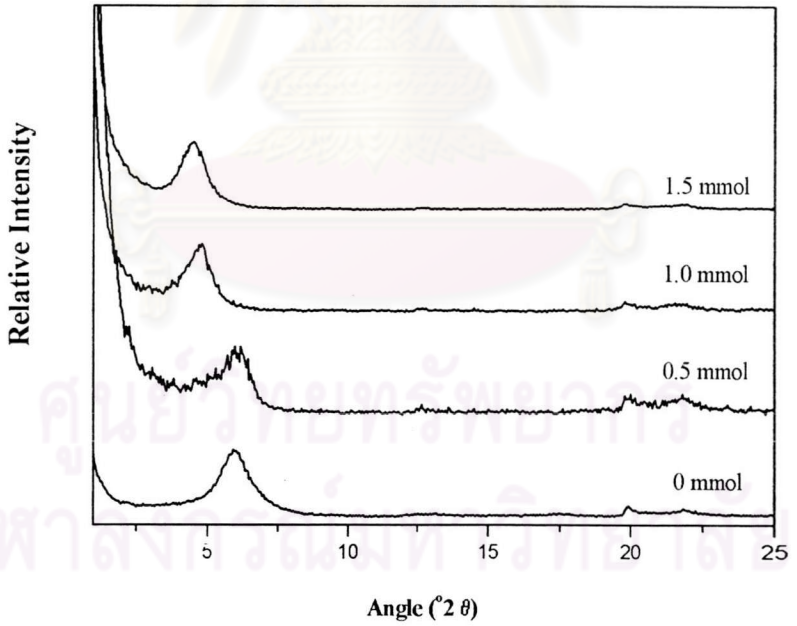

Figure 4.5 XRD patterns of TTM-BNH with various surfactant concentration loadings; 0, 0.5, 1.0, 1.5 mmol

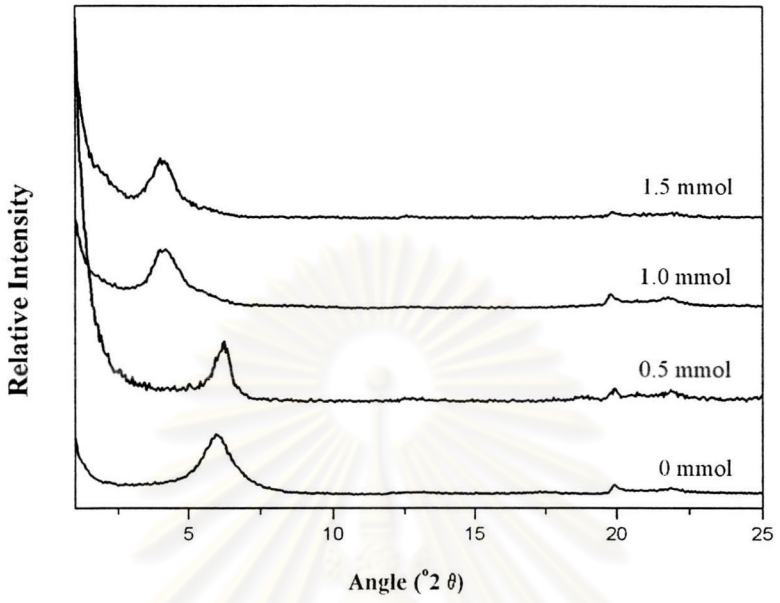

Figure 4.6 XRD patterns of OMH-BNH with various surfactant concentration loadings; 0, 0.5, 1.0, 1.5 mmol

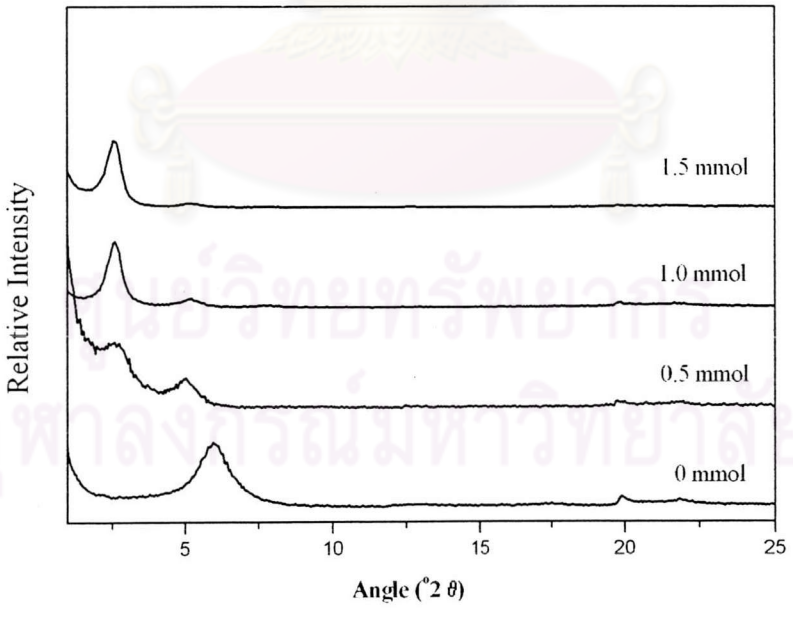

Figure 4.7 XRD patterns of ODMH-BNH with various surfactant concentration loadings; 0, 0.5, 1.0, 1.5 mmol

Table 4.4 The basal spacing of organoclay with various surfactant concentration loadings

Concentration of surfactant (mmol)	Surfactant-BNH					
	TTM-BNH		OMH-BNH		ODMH-BNH	
	d-spacing (Å)	Δd (Å)	d-spacing (Å)	Δd (Å)	d-spacing (Å)	Δd (Å)
0.0	14.01	4.01	14.01	4.01	14.01	4.01
0.5	14.66	4.66	14.18	4.18	32.48	22.48
1.0	19.37	9.37	21.07	11.07	33.89	23.89
1.5	20.03	10.03	21.15	11.15	33.61	23.61

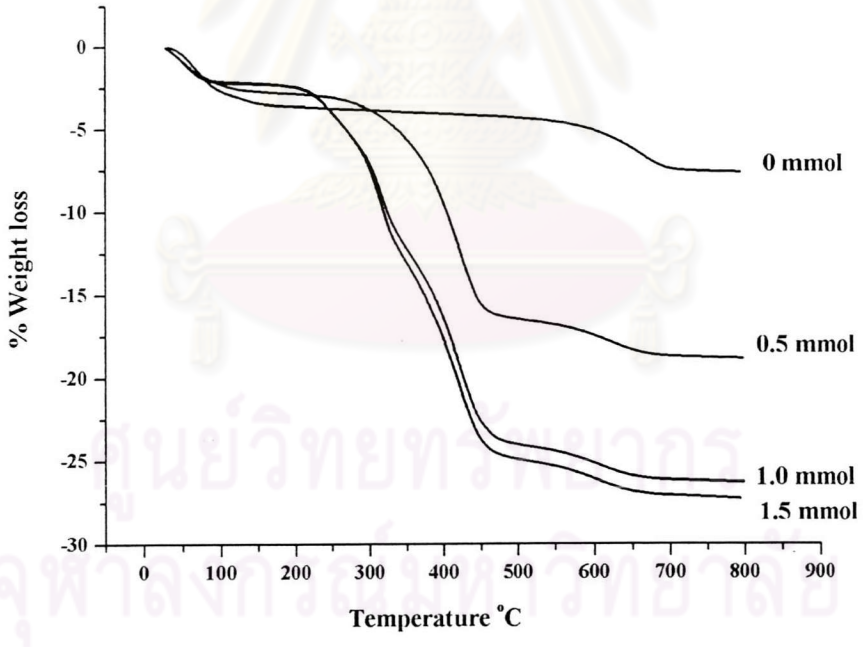

Figure 4.8 TGA thermogram of TTM-BNH with various surfactant concentration loadings; 0, 0.5, 1.0, 1.5 mmol

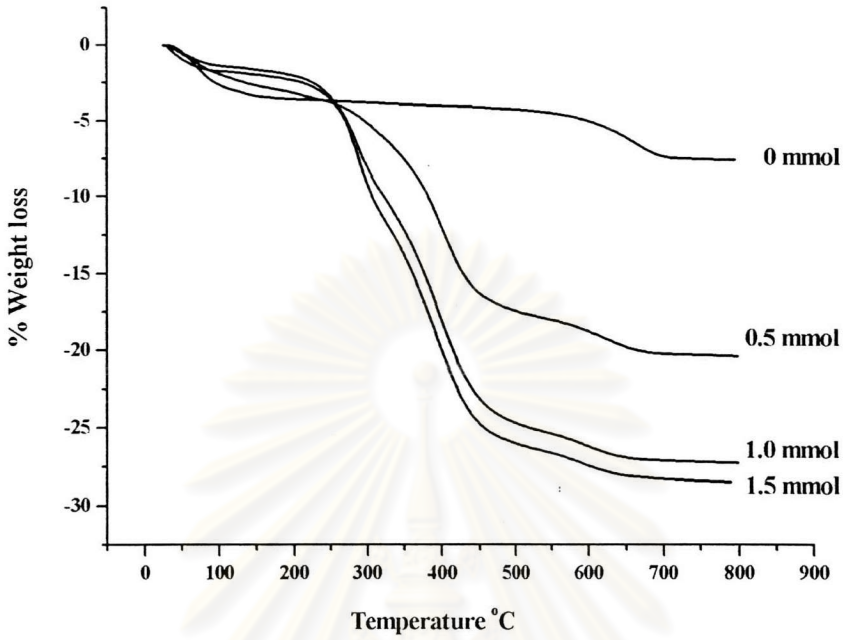

Figure 4.9 TGA thermogram of OMH-BNH with various surfactant concentration loadings; 0, 0.5, 1.0, 1.5 mmol

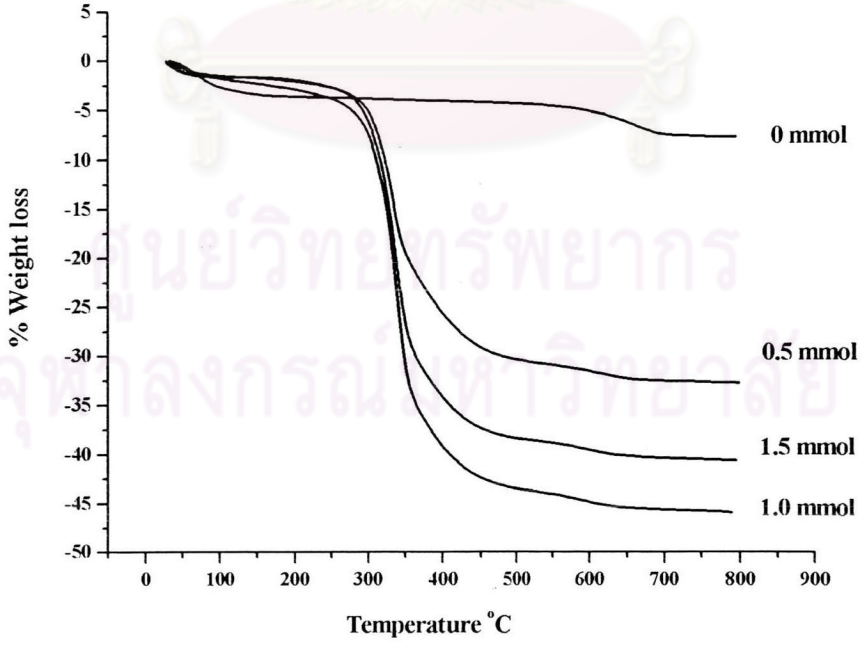

Figure 4.10 TGA thermogram of ODMH-BNH with various surfactant concentration loadings; 0, 0.5, 1.0, 1.5 mmol

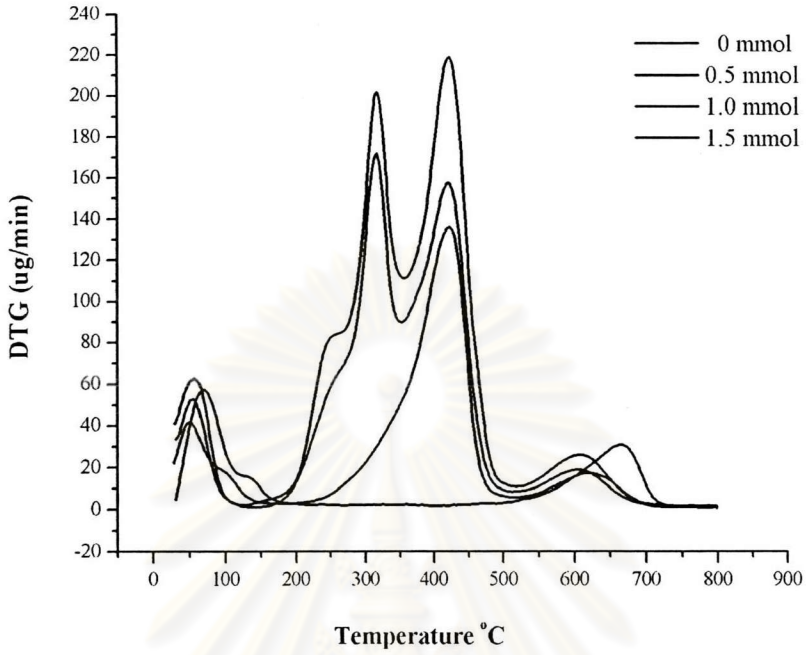

Figure 4.11 DTG thermogram of TTM-BNH with various surfactant concentration loadings; 0, 0.5, 1.0, 1.5 mmol

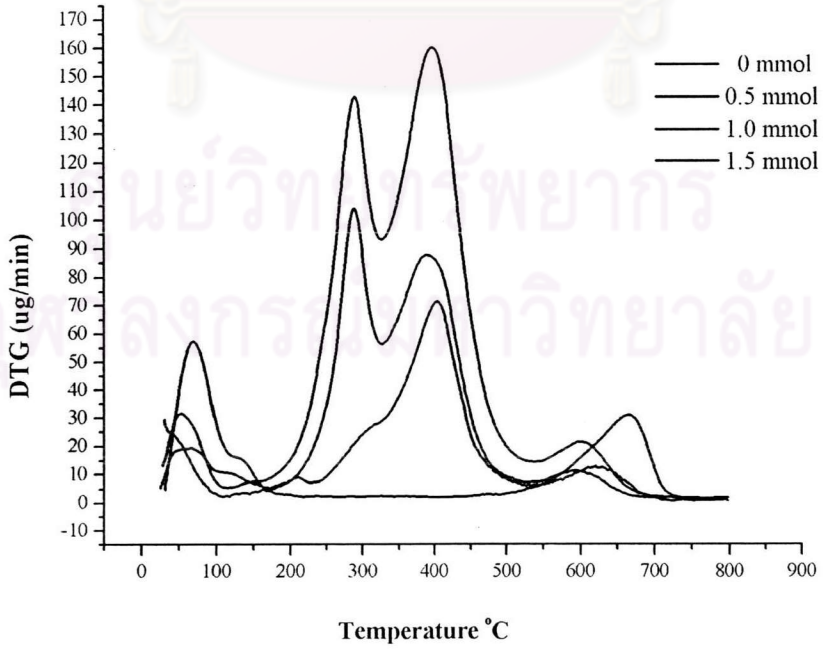

Figure 4.12 DTG thermogram of OMH-BNH with various surfactant concentration loadings; 0, 0.5, 1.0, 1.5 mmol

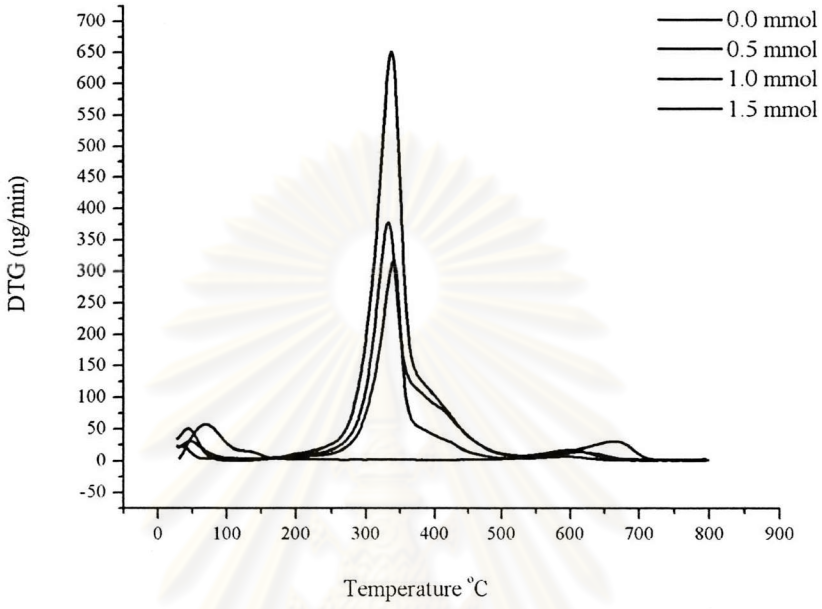

Figure 4.13 DTG thermogram of ODMH-BNH with various surfactant concentration loadings; 0, 0.5, 1.0, 1.5 mmol

Table 4.5 The calculated weight loss, % absorption, and spacing for TTM-BNH

Surfactant loading (mmol)	% Weight loss				TTM loss in mmol	% Absorption	Interlayer spacing (Å)
	Total	Water	Dehydro -xylation	TTM			
0	7.58	3.60	3.98	0.00	0.00	-	4.01
0.5	18.83	3.16	3.50	12.17	0.45	90.88	4.66
1.0	26.27	2.87	3.18	20.22	0.83	83.11	9.37
1.5	27.24	2.83	3.13	21.27	0.89	59.06	10.03

Table 4.6 The calculated weight loss, % absorption, and spacing for OMH-BNH

Surfactant loading (mmol)	% Weight loss				OMH loss in mmol	% Absorption	Interlayer spacing (Å)
	Total	Water	Dehydro -xylation	OMH			
0	7.58	3.60	3.98	0.00	0.00	-	4.01
0.5	20.38	3.10	3.43	13.85	0.44	88.09	4.18
1.0	27.26	2.83	3.13	21.29	0.74	74.12	11.04
1.5	28.49	2.79	3.08	22.62	0.80	53.41	11.15

Table 4.7 The calculated weight loss, % absorption, and spacing for ODMH-BNH

Surfactant loading (mmol)	% Weight loss				ODMH loss in mmol	% Absorption	Interlayer spacing (Å)
	Total	Water	Dehydro -xylation	ODMH			
0	7.58	3.60	3.98	0.00	0.00	-	4.01
0.5	32.67	2.62	2.90	27.15	0.39	78.95	22.48
1.0	45.90	2.11	2.33	41.46	0.75	75.03	23.89
1.5	40.60	2.31	2.56	35.73	0.59	39.26	23.61

Thermograms and %weight loss of Na-BNH and organoclay were shown in Figures 4.8-4.13 and Tables 4.5-4.7, respectively. For Na-BNH, the loss free water, situates between the clay particles, is around 100 °C. Rapid loss of (OH), dehydroxylation, takes place at around 500 °C to 750 °C.[5]

The XRD of TTM-BNH shows an increased in interlayer spacing as the TTM concentration is increased. The d-spacing is increased from 14.66 to 19.37 Å when the TTM loading is varied from 0.5 to 1 mmol/g of clay, respectively (figure 4.5). The difference in the interlayer spacing is due to the different in orientation of the interlayer TTM. The higher the d-spacing requires a closer packing of the organic molecule. The weight loss of the TTM-BNH organoclay shows two distinct weight loss events. The lost of water shows at around 100 ^{o}C and the lost of interlayer TTM shows at around 250-700 ^{o}C. The amounts of weight loss are tabulated in Table 4.5. The measured weight loss is increased as the surfactant loading is increased. This is consistent with the proposed model of the closer packing TTM. The amount of the surface coverage is closely related to the organoclay surface wettability, which is the most profound parameter in preparing the nanocomposites. An exact orientation of the interlayer surfactant is beyond the scope of this study and will not be discussed.

Similar results were observed for the OMH and ODMH case. For the OMH, the increased in the d-spacing is observed as the function of the surfactant loading. The amount of the absorbed surfactant is increased from 14 to 23% as the OMH loading increased from 0.5 and 1.0 mmol. At this point, the clay surface may be fully covered; therefore, no space is available for a further absorption. It is also possible that there might be a formation of supramolecular structure by the surfactant, which will affect the intercalation.

4.3 Dispersion of Organoclay in MMA Monomer

As mentioned in the previous section that the surface coverage and its chemistry have a profound effect on the dispersion of the organoclay. This part is intended to find the most suitable condition for the preparation of MMA-organoclay dispersion.

Dispersion of organoclay in MMA monomer is shown in Table 4.8. The dispersion is characterized as

- sedimentation: the least desirable (the organoclay surface is incompatible with the monomer),

- swelling: acceptable but not desirable (the organoclay surface is partially dispersed in the monomer) and

- suspension: the most desirable condition (most of the organoclays are fully dispersed in the monomer)

judging from its appearance (Figure 4.14).

A dispersion of Na-BNH in MMA monomer appears as the precipitate. This suggests that there is an aggregation of the Na-BNH in macroscopic scale due to an incompatibility between the Na-BNH and MMA monomer. As expected, the surface modification of clay by various surfactant types is resulting in a different dispersion of MMA monomer. All the organoclay prepared in this step will be used for the preparation of the PMMA/clay nanocomposites.

Table 4.8 The dispersion property of organoclay in MMA monomer

Organoclay	Concentration of surfactant	Observation dispersion
Na-BNH	0.0	Sedimentation
TTM-BNH	0.5	Swelling
	1.0	Swelling
	1.5	Swelling
OMH-BNH	0.5	Sedimentation
	1.0	Swelling
	1.5	Swelling
ODMH-BNH	0.5	Swelling
	1.0	Suspension (form gel)
	1.5	Suspension (form gel)

Figure 4.14 The observation of dispersion: (a) sedimentation, (b) swelling and (c) suspension

4.4 Preparation of PMMA/Clay Nanocomposite and Characterization

To elucidate the effect of the organoclay on the preparation of PMMA/clay nanocomposites, the organoclay 1.0 mmol surfactant loading was used as the reinforced material. Prepolymerization and polymerization were carried out at 60°C with 0.0018 wt.% AIBN and 110°C with 0.038 wt.% ADVN, respectively. The appearance of the PMMA/clay nanocomposites can be related to the dispersion of the organoclay in the MMA monomer (Figure 4.15).

PMMA-ODMHBNH was prepared by using ODMH-BNH, which shown the best compatibility with the MMA monomer, forming almost transparent suspension. A more detail investigation on the dispersion of nanocomposites was characterized by XRD and TEM.

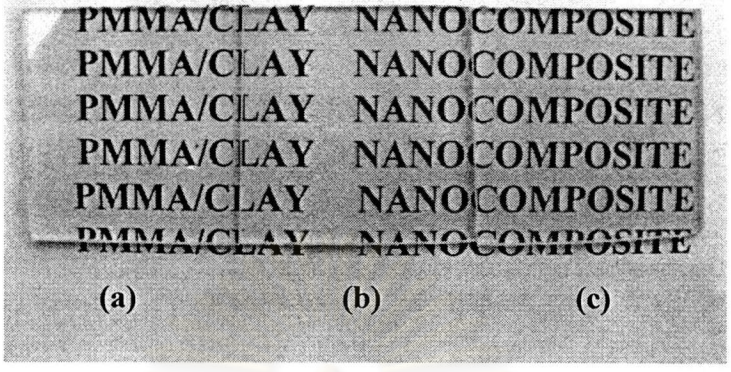

Figure 4.15 The image of PMMA/clay nanocomposite with 2% organoclay loading; a) PMMA-TTMBNH, b) PMMA-OMHBNH and c) PMMA-ODMHBNH

The XRD patterns of the PMMA/clay nanocomposites prepared in this study formed different organoclay were shown in Figures 4.16-4.18. Both TTM-BNH and ODMH-BNH sharing a feature where the absence of d001-difractionpeak was observed. This may be due to a formation of an exfoliated nanocomposites, where no crystallographic register along z-axis can be observed. It is also possible that the spacing is larger than the detection limit of the XRD used in this study, at 88 Å. An exact type dispersion will be elucidated from TEM experiment.

Figure 4.17 shows the XRD pattern of PMMA-OMHBNH. A shoulder at around $2\theta = 2.3^{o}$. These suggest that PMMA-OMHBNH is forming the intercalated clay nanocomposites. OMH-BNH shows a relative good dispersion because only the shoulder was observed by XRD.

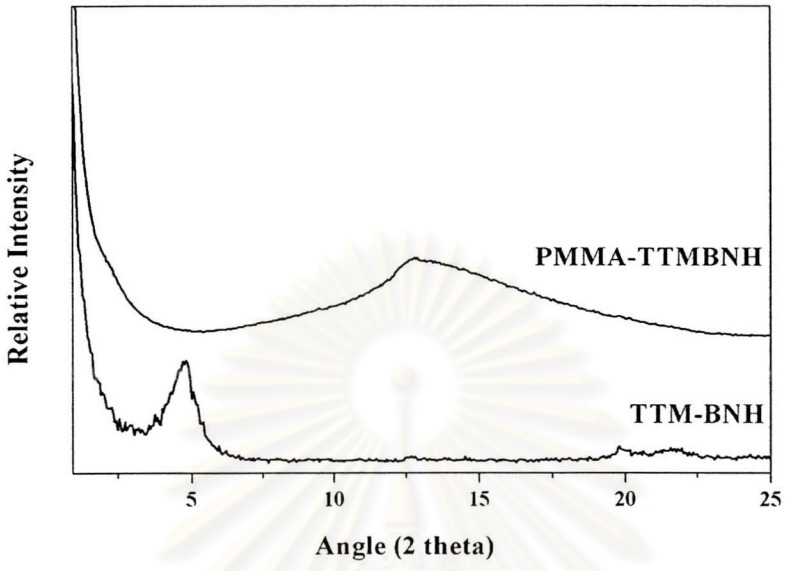

Figure 4.16 XRD patterns of organoclay and PMMA/clay nanocomposite; TTM-BNH and PMMA-TTMBNH with 2% organoclay loading

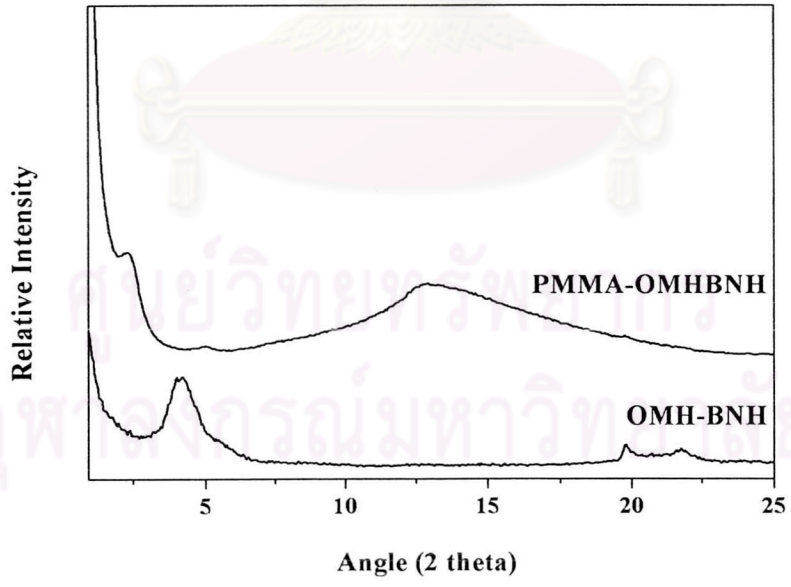

Figure 4.17 XRD patterns of organoclay and PMMA/clay nanocomposite; OMH-BNH and PMMA-OMHBNH with 2% organoclay loading

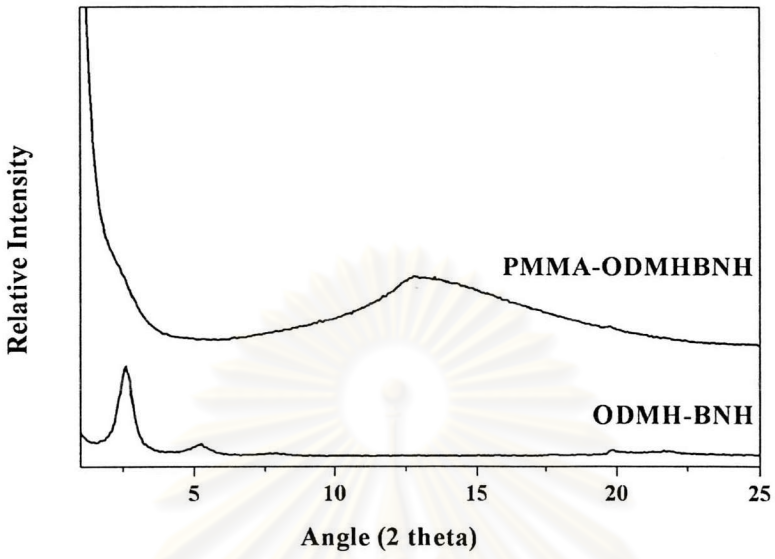

Figure 4.18 XRD patterns of organoclay and PMMA/clay nanocomposite; ODMH-BNH and PMMA-ODMHBNH with 2% organoclay loading

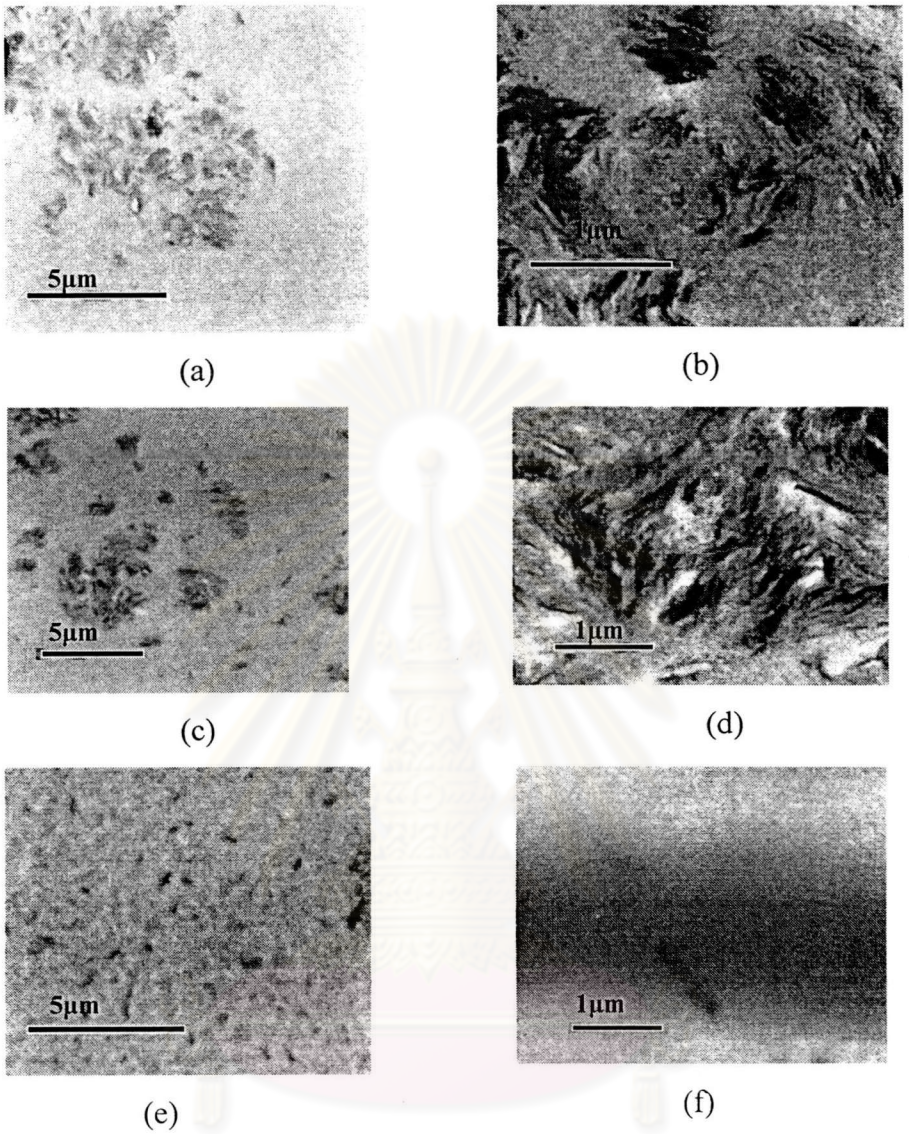

Figure 4.19 TEM image of PMMA/clay nanocomposite with 2% organoclay loading; (a), (b) PMMA-TTMBNH, (c), (d) PMMA-OMHBNH and (e), (f) PMMA-ODMHBNH

4.5 Study effect of organoclay loading in PMMA/clay nanocomposite

The image observation of PMMA/clay nanocomposite with organoclay loading of 2, 4 and 6 %wt were shown in Figure 4.20. This image illustrated that the PMMA/clay nanocomposite sheet reduced clearly, when increase the content of organoclay. For the same loading of each organoclay, the PMMA-ODMHBNH has clear optical than the other PMMA/clay nanocomposties.

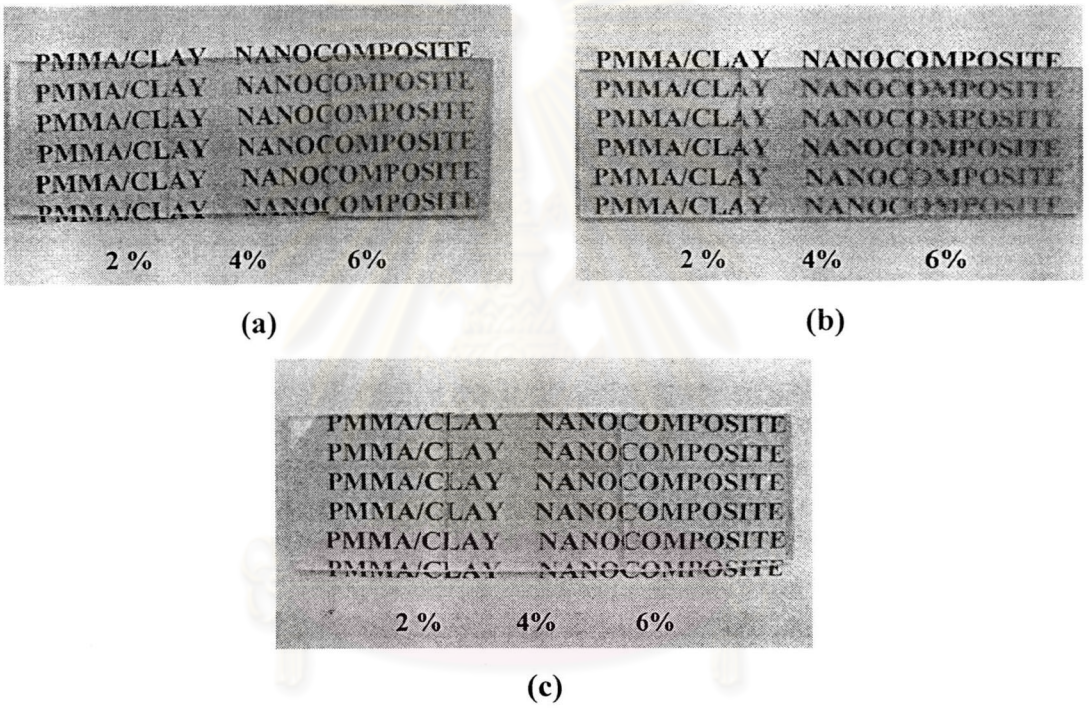

Figure 4.20 Image of PMMA/Clay nanocomposite at various organoclay loadings; (a) PMMA-TTMBNH, (b) PMMA-OMHBNH and (c) PMMA-ODMHBNH

The XRD patterns of PMMA/clay nanocomposites with organoclay loading of 2, 4 and 6 %wt were shown in Figures 4.21-4.23. The XRD patterns of PMMA-TTMBNH in Figure 4.21 absent the peak of interlayer spacing when increase the content of organocclay. The XRD peak of PMMA-OMHBNH shown height peak at $2\theta = 2.3^{\circ}$ increased, when the organoclay loading was increased. It means that the silicate layer occurred an aggregated when increased the content of organoclay. For

PMMA-ODMHBNH, there was the shoulder peak appearing, when the organoclay loading was increased. These revealed the presence of the silicate layer excited in an intercalated form. This was further confirmed by TEM micrograph shown in Figure 4.24. It was identified that there was a small amount of silicate layer that could not exfoliated in the PMMA, but dispersed in an intercalated form.

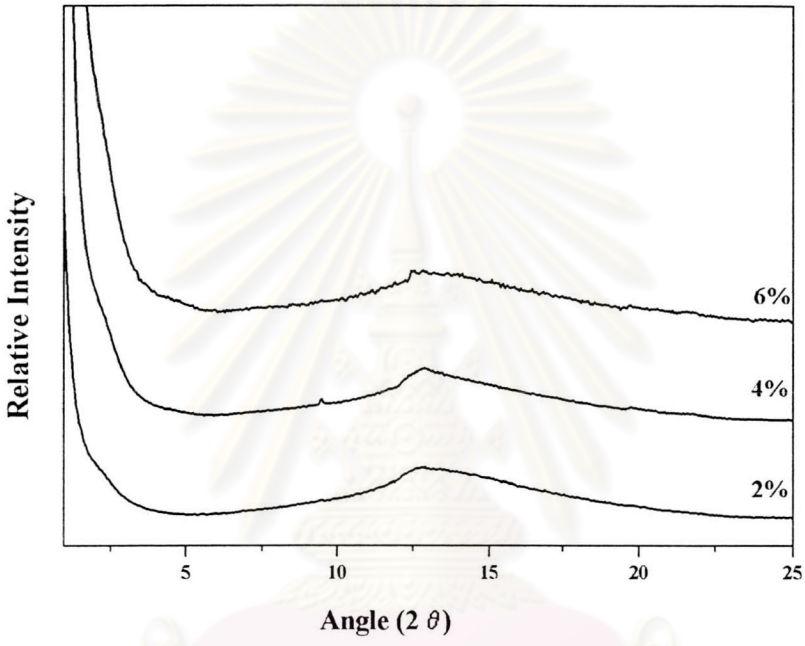

Figure 4.21 XRD patterns of PMMA-TTMBNH at various organoclay loadings

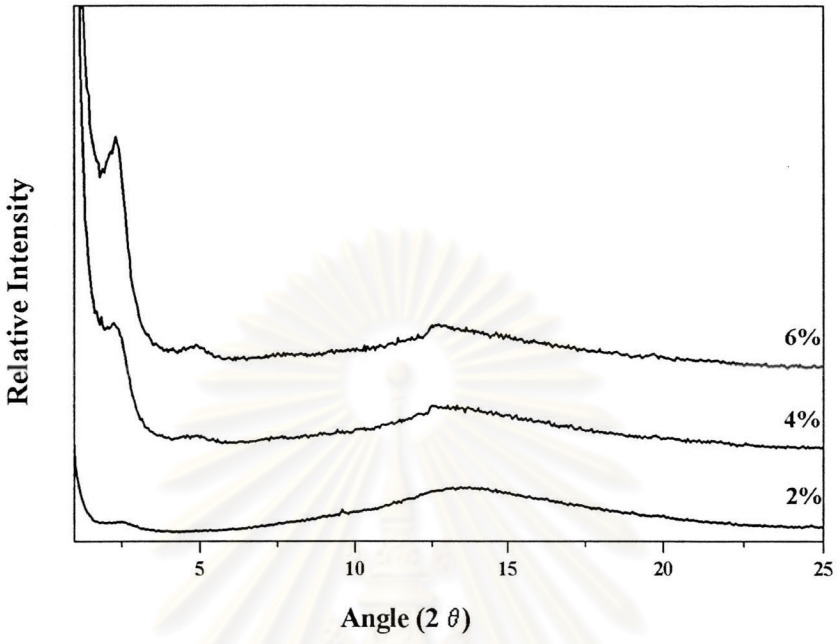

Figure 4.22 XRD patterns of PMMA-OMHBNH at various organoclay loadings

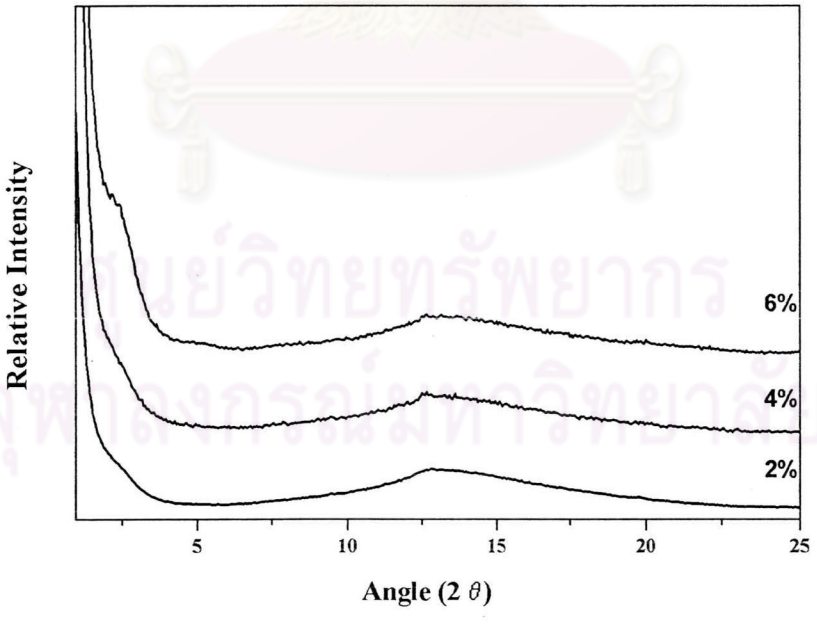

Figure 4.23 XRD patterns of PMMA-ODMHBNH at various organoclay loadings

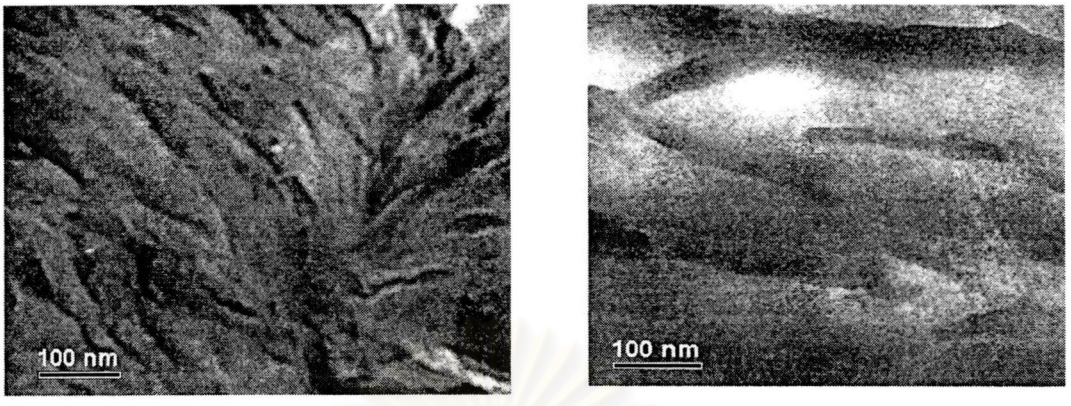

(a) (b)

Figure 4.24 TEM image of PMMA/clay nanocomposites with 6% organoclay loading; a) PMMA-TTMBNH and b) PMMA-OMHBNH

4.6 Mechanical Property

The effect of the organoclay on the mechanical properties for the selected colored PMMA/clay sheet was investigated by observation of the surface hardness and impact resistant of samples.

4.6.1 Surface Hardness

Surface hardness of the samples was measured using the Rockwell hardness tester in scale-M unit (ball indenter with 0.25 inch diameter and load at 100 kg). According to Figure 4.25, the observed surface hardness for PMMA and PMMA/clay nanocomposite was ranged from 90 to 100 in scale-M. The result suggested that the organoclay loading have the slightly effect on the surface hardness of the PMMA/clay nanocomposite casted sheets.

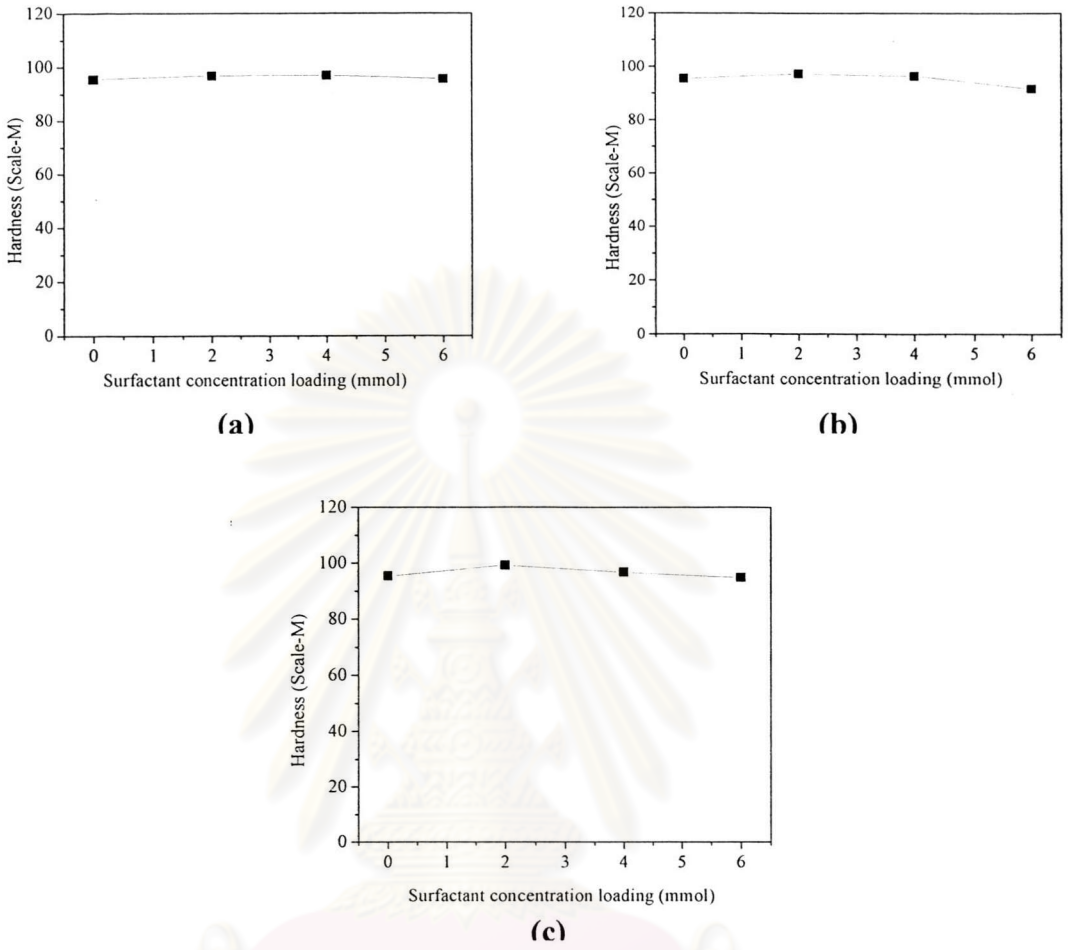

Table 4.25 Surface hardness of PMMA and PMMA/clay nanocomposite; a) PMMA-TTMBNH, b) PMMA-OMHBNH and c) PMMA-ODMHBNH

4.6.2 Impact

Impact resistance of the samples was measured using Zwick pendulum impact tester followed the ASTM D256. Figure 4.26 shows Izod impact toughness of PMMA/clay nanocomposite as function of clay loading. It was observed that the preserve of nanoclay particles also caused reduction in impact. This result was consistent with Park and Jana (2003) who reported the value of impact of PMMA/clay nanocomposite decrease when compare with PMMA.[42]

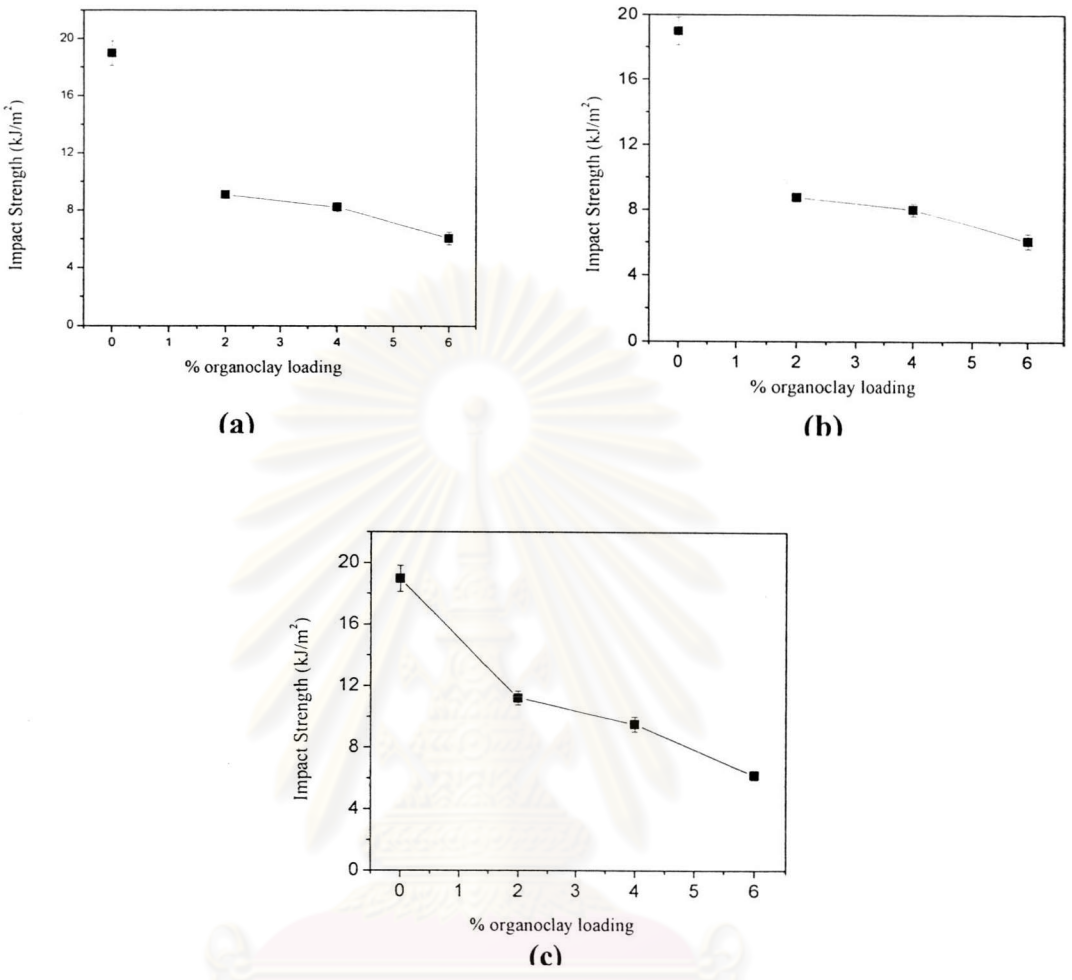

Table 4.26 Impact strength of PMMA and PMMA/clay nanocomposite; a) PMMA-TTMBNH, b) PMMA-OMHBNH and c) PMMA-ODMHBNH

4.7 Thermal property

DSC curves of the pure PMMA and PMMA/clay nanocomposite are show in Figure 4.27. The pure PMMA exhibits a heat flow charge at approximately 106 °C, corresponding to the glass transition temperature (T_g) of PMMA. Nevertheless, the PMMA/clay nanocomposites show a much higher T_g about 117-118 °C. This ascribed to the confinement of intercalated PMMA chain with in the silicate layer that prevents the segmental motion of polymer chain.

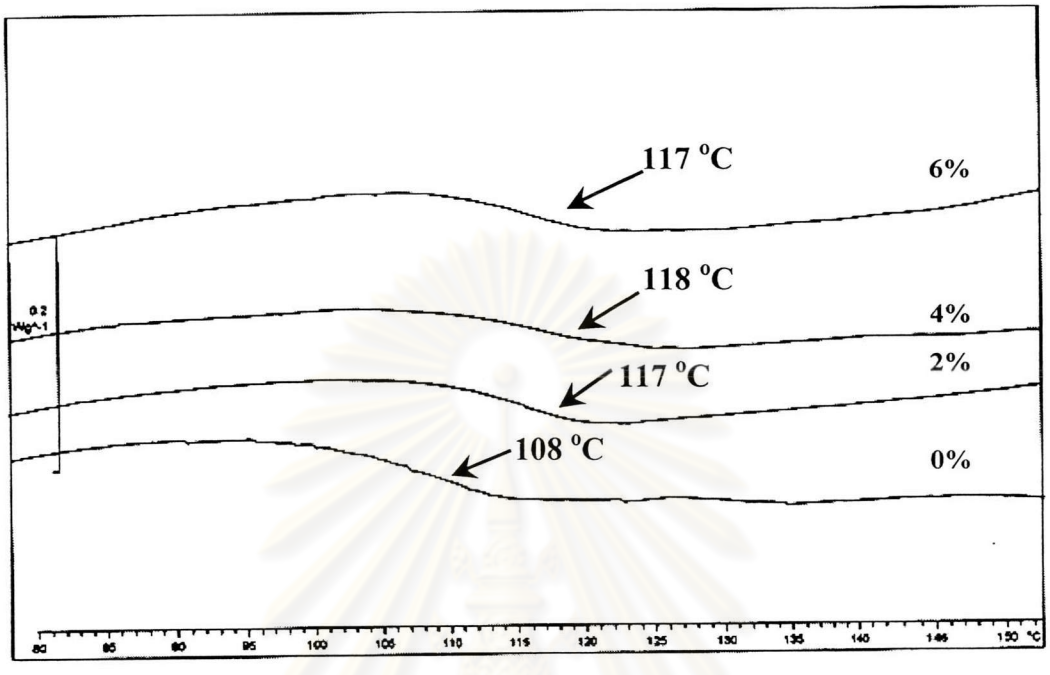

Figure 4.27 DSC curves of PMMA-ODMHBNH with various organoclay loading